MRI traceability of superparamagnetic iron oxide nanoparticle-embedded chitosan microspheres as an embolic material in rabbit uterus

Sun Young Choi, Byung Kook Kwak, Hyung Jin Shim, Jaehwi Lee, Soon Uk Hong, Kyung Ah Kim

PURPOSE
We aimed to compare polyvinyl alcohol (PVA) particles with calibrated superparamagnetic iron oxide (SPIO) nanoparticle-loaded chitosan microspheres in a rabbit model, specifically regarding the relative distribution of embolic agents within the uterus based on magnetic resonance imaging (MRI) and pathological evaluation.

METHODS
Twelve New Zealand white rabbits underwent uterine artery embolization using either standard PVA particles (45–150 μm or 350–500 μm) or calibrated SPIO-embedded chitosan microspheres (45–150 μm or 300–500 μm). MRI and histopathological findings were compared one week after embolization.

RESULTS
Calibrated SPIO-loaded chitosan microspheres 45–150 μm in size were detected on T2-weighted images. On histological analysis, calibrated SPIO-embedded chitosan microspheres were found in both myometrium and endometrium, whereas PVA particles were found only in the perimyometrium or extrauterine fat pads. A proportional relationship was noted between the calibrated SPIO-embedded chitosan microsphere size and the size of the occluded artery.

CONCLUSION
Calibrated SPIO-embedded chitosan microspheres induced greater segmental arterial occlusion than PVA particles and showed great potential as a new embolic material. SPIO-embedded chitosan microspheres can be used to follow distribution of embolic particles through MRI studies.

From the Department of Radiology and Medical Research Institute (S.Y.C. ✉ medmath@hanmail.net), Ewha Womans University School of Medicine, Seoul, Republic of Korea; the Department of Radiology (B.K.K., H.J.S.), Chung-Ang University College of Medicine, Seoul, Republic of Korea; the College of Pharmacy (J.L.), Chung-Ang University, Seoul, Republic of Korea; the Department of Maritime Medicine (S.U.H.), Maritime Medical Center, Jinhae, Republic of Korea; the Department of Radiology (K.A.K.), St. Vincent's Hospital, The Catholic University of Korea, Suwon, Republic of Korea.

Choosing a suitable embolic material is important for the successful performance of embolotherapy. Unfortunately, no single embolic material is available for use in all embolization procedures. Accordingly, the biodegradability, contour (irregular or spherical), porosity, elasticity, and other characteristics of individual embolic materials may influence the efficacy of an embolization procedure.

Uterine fibroid embolization (UFE) is a therapeutic option in the management of symptomatic fibroids (1). Even though polyvinyl alcohol (PVA) particles are the most commonly utilized embolic material in UFE, their irregular shape and large granulometric size range may lead to clogs in the catheter or proximal portion of the target vessels. This may lead to incomplete occlusion of the target vessels and unpredictable outcomes. To overcome this disadvantage, spherically shaped embolic materials were developed, including Embozene (CeloNova BioSciences, Newnan, Georgia, USA), Embosphere (Biosphere Medical, Rockland, Massachusetts, USA), Bead Block (Biocompatibles, Farnham, England), and Contour SE (Boston Scientific, Natick, Massachusetts, USA) microspheres. Because of their improved size calibration, these embolic materials were anticipated to provide more predictable and more controlled targeted vessel occlusion of a more complete and permanent nature. However, Contour SE (Boston Scientific) microspheres have not been commonly used for embolotherapy because they fail to maintain their spherical shape after embolization (2). The other commercial spherically shaped embolic products are not commonly used because of their high cost.

Accordingly, we investigated the use of chitosan microspheres as a new embolic material because they are available at a more competitive price and may offer more predictable and controlled target vessel occlusion. Chitin is a natural biopolymer obtained from the exoskeleton of crustaceans, and chitosan is obtained mainly from the deacetylation of chitin (3, 4). Chitosan can be easily formed into a spherical shape, and its safety and effectiveness as an embolic material has been demonstrated in a previous experimental study (3). The uniform size and spherical shape of chitosan make it possible for the material to penetrate more deeply into the blood vessels, without passing through the capillaries (5, 6). Chitin is biodegradable and chitin-based embolic microspheres were shown to be absorbed approximately 24 weeks after embolization of rabbit renal arteries, similar to PVA particles (3).

We chose the rabbit uterus for the embolization procedure. Rabbit uterus consists of different layers, including the endometrium, myometrium, perimyometrium, and extrauterine fat pad. Therefore, proportional distribution could be well presented according to different sizes of the embolic material. To determine the distribution of chitosan, we

took advantage of superparamagnetic iron oxide nanoparticles (SPIOs), MRI contrast agents which can be embedded within embolic materials for easier tracing with MRI (7, 8).

To date, the exact location and distribution of embolic materials at lesion sites have yet to be elucidated, although CT and MRI are frequently performed to assess the outcomes of embolotherapy. Whether MRI can trace embolic materials at lesion sites and how much of the delivered embolic material can be found at targeted lesions have yet to be meticulously studied. Accordingly, the aim of this study was to determine the traceability of SPIO-embedded chitosan microspheres of two size ranges *in vivo* in rabbit uteri and compare it with that of PVA particles of similar sizes.

Methods

Study animals

All experiments were approved by the Institutional Animal Care and Use Committee of our institution (CAUMD 10-1020) and were performed according to facility regulations on animal care and experiments. Thirteen adult female New Zealand white rabbits were used for these experiments. We divided twelve rabbits into four equal groups of three rabbits each. As uterine artery embolic materials, calibrated SPIO-embedded chitosan microspheres of two granulometric size ranges, 45–150 μm (Group I) and 300–500 μm (Group II), were compared with PVA particles (Contour, Boston Scientific) of similar sizes, 45–150 μm (Group III) and 350–500 μm (Group IV). In addition, one adult female New Zealand white rabbit was used to determine the normal anatomical features on angiography and MRI, and perform histopathologic evaluation.

Embolic materials

Glutaraldehyde (25% aqueous biological grade), chitosan (84% deacetylated, obtained from crab), tris (hydroxymethyl) aminomethane, sorbitan sesquioleate, iron standard solution for ICP (10,000 μg/mL of Fe in 4.2% [w/w] HNO_3) and hydrochloride, were purchased from Sigma–Aldrich, St. Louis, Missouri, USA. Suspension status Feridex IV (ferumoxides injectable solution;

dextran-coated SPIOs, core size of 5 nm, hydrodynamic size of 80–150 nm) was obtained, at a concentration of 3.33 mg of Fe/mL (Advanced Magnetics Inc., Cambridge, Massachusetts, USA). Acetic acid, liquid paraffin with a viscosity of 18 cP at 20°C, petroleum ether, acetone, sodium bisulfite, toluene, and other chemicals were purchased from Duksan Chemicals, Seoul, Korea. Deionized and distilled water was used to prepare all solutions. The 45–150 μm PVA and 350–500 μm PVA particles were purchased from Boston Scientific.

Preparation of SPIO-embedded chitosan microspheres

SPIO-embedded chitosan microspheres were prepared by an emulsion and cross-linking method (9). To prepare SPIO-embedded chitosan microspheres of 300–500 μm, chitosan were dissolved in 5% (v/v) acetic acid solution, and 4% (w/v) aqueous chitosan solution was prepared. About 1 mg/300 μL SPIOs emulsion were added to 3 mL of viscous chitosan solution and homogeneously dispersed. The SPIO-dispersed chitosan solution was then mixed to a mixture of petroleum ether and liquid paraffin (5:7, 30 mL) containing 3 mL of sorbitan sesquioleate, an emulsifier. To make a water-in-oil (w/o) emulsion, an overhead stirrer (IKA RW20, Fisher Scientific, Staufen, Germany) was used for the dispersion for 10 minutes at 650 rpm. Next, glutaraldehyde-saturated toluene (GST, 4 mL), which was prepared by adding glutaraldehyde (25% aqueous solution) to toluene, was mixed into the flask drop by drop and stirred for one hour. After hardening, the microspheres were washed three times with petroleum ether, one time with acetone, and three times with water. For 45–150 μm SPIO-embedded chitosan microspheres, the SPIO-dispersed chitosan solution was prepared as described above and subsequently added to a mixture of petroleum ether and liquid paraffin containing sorbitan sesquioleate. A homogenizer (IKA T18, Fisher Scientific) was used for dispersion stirrer for ten minutes at 11,000 rpm to make a w/o emulsion. GST (4 mL) was then added to the emulsion drop by drop and stirred for five minutes at 11,000

rpm. The SPIO-embedded chitosan microspheres and GST were stirred for one hour at 1000 rpm with a magnetic stirrer. The hardened microspheres were washed as described above. To prepare chitosan microspheres devoid of SPIOs, the same procedures above were performed excluding the addition of the SPIOs in an emulsion state to the chitosan solution. Before using the SPIO-embedded chitosan microspheres for the *in vivo* study, the microspheres were irradiated with ultraviolet light for 30 minutes (10).

Calibration of SPIO-embedded chitosan microspheres were made by filtering microspheres through an overlaid 45–150 μm sieve and 300–500 μm sieve (Chunggye Industrial MFG. Co., Seoul, Korea). SPIO-embedded chitosan microspheres were observed with a light microscope (BX51, Olympus Optical, Tokyo, Japan) to confirm embedment.

Preparation of MRI phantoms

Polysaccharide agarose powder (Bacto™, BD Biosciences, Franklin Lakes, New Jersey, USA) was suspended in distilled water at a 5% (w/v) concentration in a glass beaker under constant stirring at room temperature. The beaker was then boiled until the agarose was dissolved. After cooling this solution to <40°C, prepared embolic materials were added to the solution at a ratio of 0.1 to 4.9 mL (v/v); i.e., 45–150 μm SPIO-embedded chitosan microspheres, 300–500 μm SPIO-embedded chitosan microspheres, 45–150 μm PVA particles, or 350–500 μm PVA particles, respectively. These where then stirred until evenly distributed, transferred to 10 mL tubes, and allowed to cool until they formed a gel.

To determine whether SPIO-embedded chitosan microspheres can be observed by MRI, four of the above-described tubes were placed in one line in a rack. MRI was performed with a 3.0 Tesla whole-body scanner (Philips Achieva, Philips Medical Systems, Best, The Netherlands) with a head array coil comprising the following sequences: (i) T2-weighted turbo spin-echo imaging (repetition time, 3000 ms; echo time, 100 ms; thickness, 0.8 mm; field of view (fov) 150×150; flip angle, 90°) and (ii) T2*-weighted gradient echo imaging (repetition time, 700 ms; echo

time, 9.6 ms; thickness, 0.5 mm; fov, 150×150; flip angle, 30°).

Angiography and embolization protocol

Uterine arterial embolization was performed in 12 New Zealand white rabbits weighing 3.6±0.7 kg each. To induce anesthesia, 5 mg/kg of tiletamine/zolazepam (Zoletil 50, Virbac, Seoul, Korea) and 2.5 mg/kg of xylazine (Rompun, Bayer Korea, Seoul, Korea) were intravenously injected. A 4 F vascular sheath (Pinnacle R/O introducer sheath, Terumo, Tokyo, Japan) was then inserted into the left carotid artery by surgical cutdown. Next, a 2 F microcatheter (Progreat α, Terumo) was advanced via vascular sheath and positioned in the distal abdominal aorta for initial nonselective pelvic angiography. Bilateral uterine arteries were then selected with a 2 F microcatheter (Progreat α, Terumo), individually. After selective catheterization of the bilateral uterine arteries, uterine artery angiography was carried out to enable identification of the vasculature and parenchyma of the uterus. Embolization was performed in free flow: 0.1 mL of each embolic material (PVA particles and calibrated SPIO-embedded chitosan microspheres) was suspended in 4.9 mL of a mixture of iodinated contrast medium (Visipaque, GE Healthcare, Princeton, New Jersey, USA) and normal saline (1:1, v/v); this mixture was diluted to a concentration, 3.5 to 4.0 times lower than that used in clinical practice (11).

To maintain homogeneous suspension of the particles, the mixture was agitated before each injection. The mixture was injected slowly under fluoroscopic guidance, using 1 mL Luer Lock syringes. Approximately 2 mL of saline was pushed into the microcatheter after each injection. When proximal arterial flow was greatly reduced under the fluoroscope, embolization was stopped. The end point was the same for all embolic materials. The procedure was applied equally for all uterine arteries. During the procedure, injectability of the particles through the microcatheter was estimated. The degree of resistance during injection was graded in consensus prior to the procedure by two interventional radiologists (B.K.K. and H.J.S. with 26 and 31 years of experience, respectively) according to the following scale: grade 0, saline-like injection; grade 1, resistance; and grade 2, catheter occlusion. The target injection grade for these procedures was grade 1 (1).

After embolization, all devices were removed and the carotid artery was tied with 3-0 silk. To prevent infection, cefazolin sodium (Cefamezin injectable, Dong-A Pharmaceutical, Seoul, Korea) was intramuscularly injected: a single dose of 100 mg/kg/day for three days after embolization.

MRI protocol

MRI for evaluation of normal anatomical features was performed in one rabbit that did not go through uterine arterial embolization. The other 12 rabbits were scheduled to undergo MRI one week after embolization. MRI examinations were performed with a 3.0 Tesla whole-body scanner (Philips Achieva, Philips Medical Systems) with a knee array coil. MRI was performed with the following sequences: (i) coronal T1-weighted turbo spin-echo imaging (repetition time, 412 ms; echo time, 10 ms; thickness, 2 mm; fov, 150×150 mm), (ii) coronal T2-weighted turbo spin-echo imaging (repetition time, 1956 ms; echo time, 100 ms; thickness, 2 mm; fov, 150×150 mm), (iii) sagittal T1-weighted turbo spin-echo imaging (repetition time, 1195 ms; echo time, 10 ms; thickness, 3 mm; fov, 120×120 mm), (iv) sagittal T2-weighted turbo spin-echo imaging (repetition time, 3773 ms; echo time, 100 ms; thickness, 3 mm; fov, 120×120 mm), (v) contrast-enhanced coronal T1-weighted turbo spin-echo imaging (repetition time, 525 ms; echo time, 10 ms; thickness, 2 mm; fov, 150×150 mm), and (vi) contrast-enhanced sagittal T1-weighted turbo spin-echo imaging (repetition time, 1232 ms; echo time, 10 ms; thickness, 3 mm; fov, 120×120 mm). About 0.2 mL/kg of gadoteric acid (Dotarem, Guerbet, Paris, France) was injected intravenously for the MRI contrast study. The flip angle was 90° through all sequences. To visualize the MRI findings of a normal uterus, the same sequences were obtained with contrast agent in one rabbit. All images obtained after the embolization procedure were compared with normal uterus images. The presence of embolization particles was assessed on T2-weighted MRI.

MRI analysis

Two radiologists (K.A.K. and S.Y.C. with nine and 10 years of experience, respectively) reviewed the images in consensus. The types of embolic materials were blinded to these two radiologists.

The MRI analyses were performed by focusing on the following findings in each group: signal change of the uterine body on T1-weighted, T2-weighted, and contrast-enhanced T1-weighted images; identification of the dark, low-signal intensity of the SPIO-embedded chitosan microspheres on T2-weighted images; any complications related to the embolization procedure on T1-weighted, T2-weighted, and contrast-enhanced T1-weighted images.

Histopathologic analysis

All rabbits were immediately sacrificed after completion of the MRI. Laparotomy along the linea alba was performed and pelvic exploration was followed. Visual inspection of the genital tract, bladder, and adjacent gastrointestinal tract was performed to evaluate the consistency of these structures among the rabbits and to identify necrosis. Next, the uterus and ovaries, including the periuterine fat pads containing the afferent arterial system, were removed. All harvested organs were routinely fixed with 10% formalin for 24 hours and processed by paraffin embedding. Four sagittal 10 mm thick sections were obtained for each proximal uterine horn, 2 cm from the internal orifice of the cervix. Standard hematoxylin-eosin staining was then performed. Evaluated parameters were followed: the presence and number of embolic materials, the distribution of the embolic materials according to the layers of the uterus (i.e., endometrium, myometrium, perimyometrium, and periuterine fat pads), and the diameter of the occluded artery. The extent of necrosis in each slice was also evaluated.

The pathologic evaluations were performed by a pathologist (S.U.H.) on all specimens using light microscopy. The pathologist was blinded to the type of embolic material used.

Statistical analysis

Statistical analysis was performed using the SPSS statistical package for Windows, version 20.0 (IBM Corp., Armonk, New York, USA). The percentage of pathologic infarction and occluded vessel diameter were analyzed using the Mann–Whitney test according to the embolic materials. A P value of <0.01 was deemed to indicate a statistically significant difference.

Results

Under light microscope, calibrated SPIO-embedded chitosan microspheres of 300–500 µm were globular or elliptical in shape and uniform in size (Fig. 1a). They were darker than the blank chitosan microspheres of 300–500 µm (Fig. 1b).

In MRI phantoms, large-sized calibrated SPIO-embedded chitosan microspheres were vaguely detected on T2-weighted images. Neither small-sized calibrated SPIO-embedded chitosan microspheres nor small- or large-sized PVA particles were detected on T2-weighted images (Fig. 2a). Both small- and large-sized calibrated SPIO-embedded chitosan microspheres were detected on T2*-weighted images; no PVA particles of any size were detected (Fig. 2b).

Uterine arterial embolization was performed in 12 rabbits. A schematic image of the uterine artery in rabbits is shown in Fig. 3a. Superselective catheterization and free-flow embolization of the bilateral uterine arteries were successfully achieved in all animals (Fig. 3b, 3c). No catheter occlusion was observed in any group. The injection grade for all procedures was grade 1. One rabbit in Group IV died suddenly of an unknown cause six days after embolization.

Postembolization MRI was performed in 11 of 12 animals, excluding the one in Group IV that died six days after embolization. MRI findings of the normal rabbit uterus showed low signal intensity on T1- and T2-weighted images and high signal intensity on contrast-enhanced T1-weighted images (Fig. 4a–c). Meanwhile, embolized uteri showed increased signal intensity on T1- and T2-weighted images and decreased enhancement on contrast-enhanced T1-weighted images (Fig. 4d–f).

Among the groups, effective signal intensity changes were noted in two rabbits in Group I, three in Group II, two in Group III, and none in Group IV (Table 1). SPIO-embedded chitosan microspheres were seen as dots of dark signal intensity on T2-weighted images (Fig. 4e).

In gross pathology, all uterine specimens in all groups showed diffuse volume shrinkage. One of the uterine specimens in Group I, three in Group II, and two in Group III showed diffuse or multifocal hemorrhagic infarction. Three specimens in Group II showed
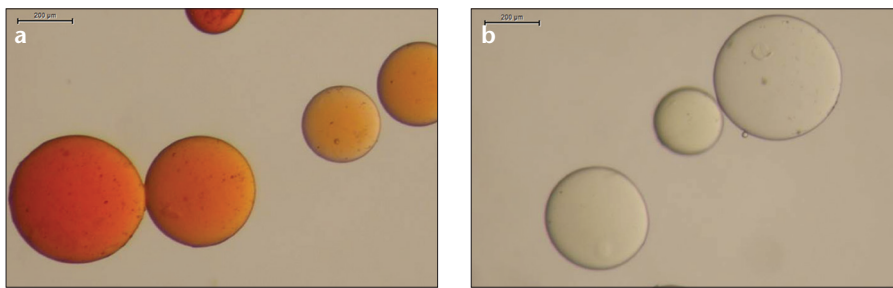
Figure 1. a, b. Light microscopic examination of calibrated SPIO-embedded 300–500 µm chitosan microspheres **(a)** and blank 300–500 µm chitosan microspheres **(b)**. Calibrated SPIO-embedded chitosan microspheres **(a)** were globular or elliptical in shape and uniform in size. The SPIO-embedded chitosan microspheres **(a)** were darker than blank chitosan microspheres **(b)**, because of the SPIOs (×200) (bar, 200 µm).
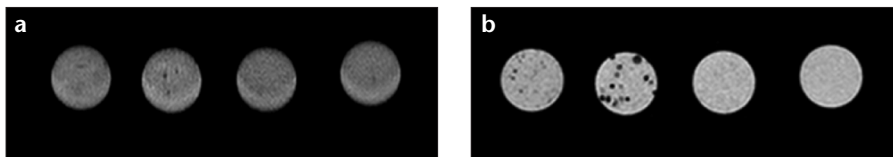
Figure 2. a, b. MRI phantoms of the four embolic materials (Groups I, II, III, and IV, from left to right) on T2- and T2*-weighted images. On axial T2-weighted image **(a)**, Group II microspheres were vaguely observable with dark signal intensity. Neither Group I microspheres, nor Group III or IV particles, were observed on T2-weighted images. On axial T2*-weighted images **(b)**, Group I and II microspheres were observed as dots of dark signal intensity; no Group III or IV particles could be seen.
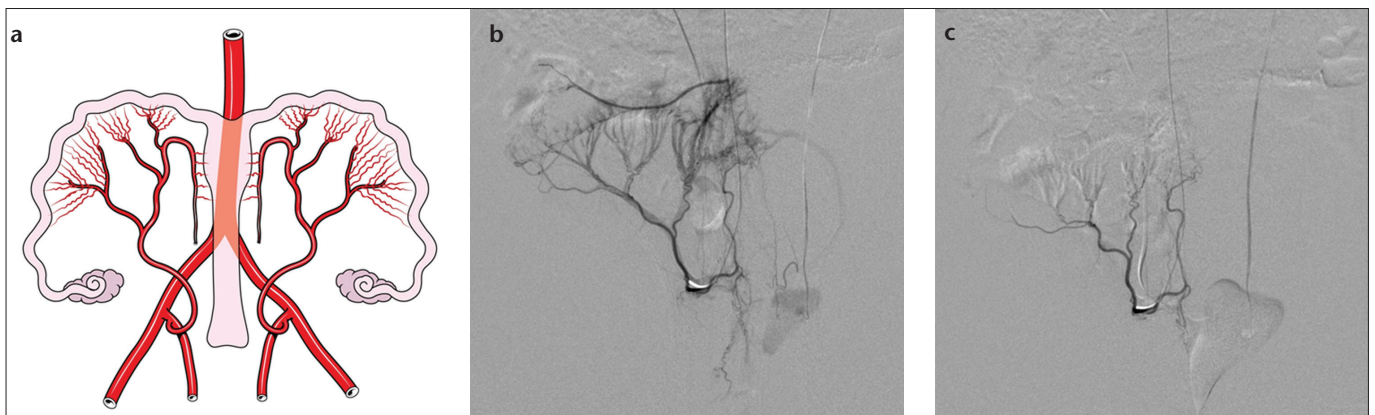
Figure 3. a–c. Selective uterine artery angiography of rabbits. Panel **(a)** shows schematic image of the uterine artery in rabbits. Selective angiography of the right uterine artery before the embolization procedure **(b)** showed multiple helicine branches feeding to the uterine body. Follow-up angiography **(c)** shows occlusion of multiple helicine branches after the embolization procedure.

Table 1. Signal change in the MRI of four groups after bilateral uterine artery embolization

MRI	Group I 1	2	3	Group II 1	2	3	Group III 1	2	3	Group IV 1*	2	3
T1	↑	–	↑	↑	↑	↑	–	↑	↑	N/A	–	–
T2	↑	↑	↑	↑	↑	↑	↑	↑	↑	N/A	↑	↑
CE-T1	↓	↓	↓	↓	↓	↓	↓	↓	↓	N/A	↓	↓
Particle (T2)	+	+	–	–	–	–	N/A	N/A	N/A	N/A	N/A	N/A

Embolic materials: Group I, SPIO-embedded chitosan microspheres (45–150 μm); Group II, SPIO-embedded chitosan microspheres (300–500 μm); Group III, PVA particles (45–150 μm); Group IV, PVA particles (350–500 μm).
N/A, not applicable; CE-T1, contrast-enhanced T1 sequence; Particle (T2), detection of embolic material on T2-weighted sequences.
*MRI was not performed in this animal because of sudden death.
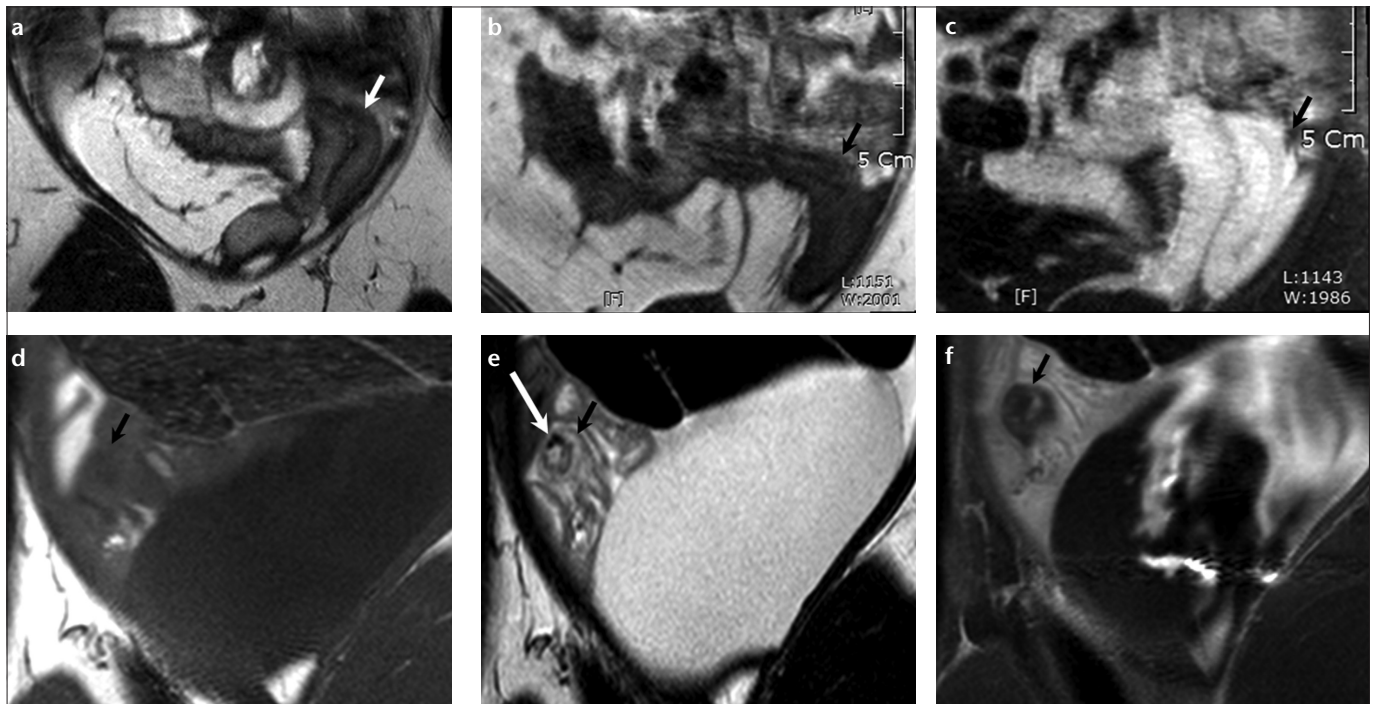
Figure 4. a–f. MRI analysis of the normal and embolized (Group I) rabbit uteri. Coronal T1-weighted image **(a)** and T2-weighted image **(b)** of the normal rabbit uterine body show low signal intensity *(arrow)*. Contrast-enhanced coronal T1-weighted image **(c)** shows bright enhancement of the normal rabbit uterine body *(arrow)*. Coronal T1-weighted image **(d)** shows intermediate signal intensity of the uterine body after embolization *(arrow)*. Coronal T2-weighted image **(e)** shows high signal intensity of the uterine body after embolization *(short arrow)*. Dots of dark signal intensity reveal the SPIO-embedded chitosan microspheres **(e,** *long arrow)*. Contrast-enhanced coronal T1-weighted image **(f)** shows decreased enhancement of the uterine body after embolization *(arrow)*.

intra-abdominal adhesion. One specimen in Group III showed combined right-sided hydronephrosis.

Histopathologic analysis of the specimens from Group I and II revealed the presence of embolic materials in the endometrium, myometrium, and perimyometrium. In contrast, no embolic material was found in the endometrium or myometrium of the specimens from Group III or IV (Figs. 5, 6). One PVA particle in a Group III specimen was found in the perimyometrium, while all other particles in Group III and IV specimens

were found in the periuterine fat pads (Figs. 5, 6). In addition, infarction ratios changed significantly with different size of SPIO-embedded chitosan microspheres used in Group I and II ($P = 0.001$); similarly, occluded vessel diameter changed significantly with different size of SPIO-embedded chitosan microspheres used in Group I and II ($P = 0.001$) (Table 2).

Discussion

In the present study, chitosan microspheres penetrated more deeply than PVA particles, and more notably, a cor-

relation was observed between the chitosan microsphere particle size and the occluded vessel diameter. In contrast, no correlation was observed between the PVA particle size and the occluded vessel diameter, and despite their small size, PVA particles failed to penetrate the uterus. In fact, most PVA particles were found outside the uterus. Based on these results, we suggest that chitosan microspheres could potentially be used as a new embolic material. Gross pathologic examination showed intra-abdominal adhesion in Group II rabbits, indicating the effectiveness of the chi-

Table 2. Comparison of pathologic infarction area and occluded vessel diameter in study groups

	Group I	Group II	P	Group III	Group IV	P
Pathologic infarction (%)	11.2±28.1	32.8±28.4	0.001	49.8±36.8	19.4±31.1	0.006
Diameter of occluded vessel (μm)	1.65±1.08	2.55±1.17	0.001	1.69±1.83	1.8±0.07	0.505

Mann-Whitney U test was used in statistical comparison.
*Data are presented as mean±standard deviation.
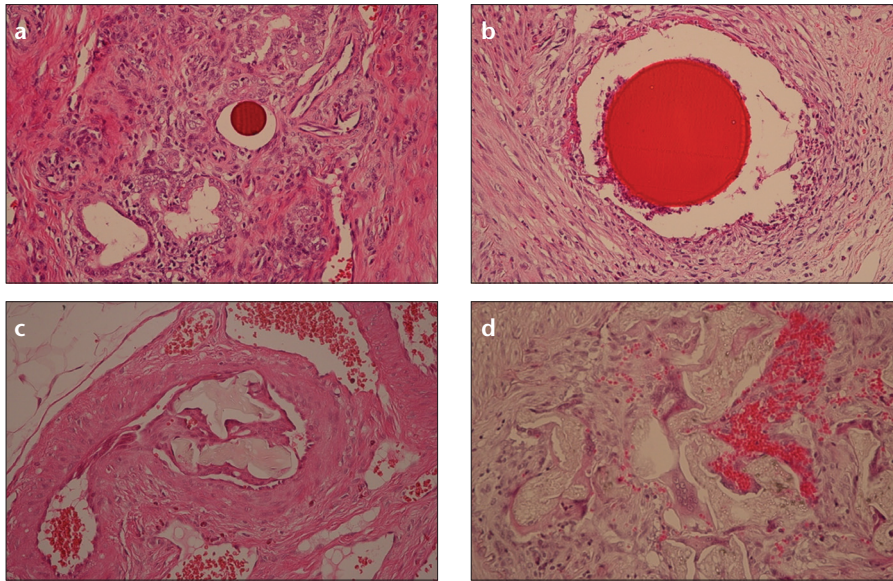
Figure 5. a–d. Photomicrographs of rabbit uterine arteries filled with various embolic materials (hematoxylin-eosin staining; original magnification, ×400). Group I **(a)** and II **(b)** SPIO-embedded chitosan microspheres are present in the arterial lumen and appear spherical and homogeneous in structure. Group I microspheres **(a)** are present in the endometrium, while Group II microspheres **(b)** are present in the myometrium. Group III **(c)** and IV **(d)** PVA particles are present in the arterial lumen in extrauterine fat pads and appear to have irregular shapes.

Figure 6. Schematic drawing of embolic material distribution as detected during the pathologic evaluation of the four groups. The number of dots is equal to the number of embolic particles found during the pathologic evaluation of each group. E, endometrium; M, myometrium; P, perimyometrium; F, extrauterine fat pad.

than thin-walled hollow viscus. We used rabbit uterus in our experimental setup, but other solid organs such as liver and kidney could be suitable for embolization using this new material. We suggest that transarterial chemoembolization, traumatic arterial bleeding in the liver, kidney, or spleen, benign tumorous conditions such as angiomyolipoma or arteriovenous malformation are suitable clinical indications for using chitosan microspheres.

The goal of UFE is to produce hemorrhagic infarction of fibroids while maintaining endometrial and myometrial perfusion (12–14). Chitosan microspheres of both size ranges were able to deeply penetrate the inner uterus. In gross pathology, the total number of embolic particles that penetrated the uterine body was higher in Group I than in Group II. However, MRI and gross pathology showed the presence of hemorrhagic infarction in all Group II uteri. In addition, a larger portion of vessels were occluded in Group II than in Group I. Accordingly, the percent infarcted area was higher and the embolization effect was superior for Group II compared with Group I. Although the percentage of pathologic infarction was highest for Group III, no definite intra-abdominal adhesion was found upon gross inspection. This may have resulted from a greater inflammatory reaction to chitosan microspheres than to PVA particles (3).

One specimen from Group III showed right-sided hydronephrosis on gross pathologic evaluation. In rabbits, the uterine artery branches off to supply the ureters, urinary bladder, and vagina. In the embolization procedure, a microcatheter tip was positioned at the ostium of the main uterine artery. Therefore, some of these branch vessels could have been occluded during the embolization procedure, which may have led to hydronephrosis after the embolization.

tosan microspheres in the embolization procedure. However, this post-procedural adhesion may produce harmful results when applied to an organ consisting of a thin parenchyma such as a hollow viscus. Therefore, we conclude that solid organs are more suitable for embolization by chitosan microspheres

After UFE, MRI is commonly used for follow-up imaging to assess the effectiveness of embolization and to identify any complications. The ability to detect an embolic material on follow-up imaging may be helpful in estimating its distribution. In this study, we embedded SPIOs in chitosan microspheres and evaluated their detectability by MRI after the embolization. The pathology results revealed that small-sized SPIO-embedded chitosan microspheres penetrated more deeply than the large-sized microspheres. In addition, a greater number of small-sized SPIO-embedded chitosan microspheres than large-sized microspheres were able to penetrate the tissue. Therefore, small-sized, SPIO-embedded chitosan microspheres may be able to form clusters deep inside the tissue, making them detectable on follow-up MRI. In the phantom study, the SPIO-embedded chitosan microspheres could be distinctly detected on T2*-weighted images and detected only vaguely on T2-weighted images. In the *in vivo* study, few small-sized SPIO-embedded chitosan microspheres could be detected on T2-weighted images. This discrepancy may have resulted from the differences between *in vivo* and *in vitro* studies. Unfortunately, clinical application of T2*-weighted images for evaluation of the uterus in humans is limited by the low spatial resolution of this technique. However, detailed adjustment of imaging parameters may allow for SPIO-embedded chitosan microspheres to be traced on T2*-weighted images.

A limitation of our study was the small number of animals used, but it is the first study to describe the use of calibrated SPIO-embedded chitosan microspheres in the embolization of rabbit uteri.

In conclusion, we showed that the calibrated SPIO-embedded chitosan microspheres allowed for more segmental arterial occlusion than that achieved with the PVA particles and showed great potential as a new embolic material, traveling more distally into blood vessels. Moreover, the level of arterial occlusion was associated with the size of the SPIO-embedded chitosan microspheres. The detection of SPIO-embedded chitosan microspheres by MRI might be of use in evaluating the distribution of embolic materials.

Acknowledgements

Conflict of interest disclosure

The authors declared no conflicts of interest.

References

1. Pelage JP, Laurent A, Wassef M, et al. Uterine artery embolization in sheep: comparison of acute effects with polyvinyl alcohol particles and calibrated microspheres. Radiology 2002; 224:436–445. [CrossRef]
2. Stampfl S, Bellemann N, Stampfl U, et al. Arterial distribution characteristics of Embozene particles and comparison with other spherical embolic agents in the porcine acute embolization model. J Vasc Interv Radiol 2009; 20:1597–1607. [CrossRef]
3. Kwak BK, Shim HJ, Han SM, Park ES. Chitin-based embolic materials in the renal artery of rabbits: pathologic evaluation of an absorbable particulate agent. Radiology 2005; 236:151–158. [CrossRef]
4. Muzzarelli R, Baldassarre V, Conti F, et al. Biological activity of chitosan: ultrastructural study. Biomaterials 1988; 9:247–252. [CrossRef]
5. Derdeyn CP, Graves VB, Salamat MS, Rappe A. Collagen-coated acrylic microspheres for embolotherapy: in vivo and in vitro characteristics. Am J Neuroradiol 1997; 18:647–653.
6. Bendszus M, Klein R, Burger R, Warmuth-Metz M, Hofmann E, Solymosi L. Efficacy of trisacryl gelatin microspheres versus polyvinyl alcohol particles in the preoperative embolization of meningiomas. Am J Neuroradiol 2000; 21:255–261.
7. Reddy AM, Kwak BK, Shim HJ, et al. In vivo tracking of mesenchymal stem cells labeled with a novel chitosan-coated superparamagnetic iron oxide nanoparticles using 3.0T MRI. J Korean Med Sci 2010; 25:211–219. [CrossRef]
8. Shi Z, Neoh KG, Kang ET, et al. (Carboxymethyl) chitosan-modified superparamagnetic iron oxide nanoparticles for magnetic resonance imaging of stem cells. ACS Appl Mater Interfaces 2009; 1:328–335. [CrossRef]
9. Jameela SR, Jayakrishnan A. Glutaraldehyde cross-linked chitosan microspheres as a long acting biodegradable drug delivery vehicle: studies on the in vitro release of mitoxantrone and in vivo degradation of microspheres in rat muscle. Biomaterials 1995; 16:769–775. [CrossRef]
10. Umeki N, Sato T, Harada M, et al. Preparation and evaluation of biodegradable microspheres containing a potent osteogenic compound and new synthetic polymers for sustained release. Int J Pharm 2010; 392:42–50. [CrossRef]
11. Abramowitz SD, Israel GM, McCarthy SM, Pollak JS, White RI Jr, Tal MG. Comparison of four embolic materials at uterine artery embolization by using postprocedural MR imaging enhancement. Radiology 2009; 250:482–487. [CrossRef]
12. Kitamura Y, Ascher SM, Cooper C, et al. Imaging manifestations of complications associated with uterine artery embolization. Radiographics 2005; 25:S119–132. [CrossRef]
13. Pelage JP, Cazejust J, Pluot E, et al. Uterine fibroid vascularization and clinical relevance to uterine fibroid embolization. Radiographics 2005; 25:S99–117. [CrossRef]
14. Jha RC, Allison SJ, Ascher SM. Uterine artery embolization & gynecologic embolotherapy. Baltimore: Lippincott Wiliams & Wilkins, 2005.